Biodesign

pISSN 2288-6982 | eISSN 2288-7105

ARTICLE P 84-91

Crystal structure of unphosphorylated Spo0F from *Paenisporosarcina* sp. TG-14, a psychrophilic bacterium isolated from an Antarctic glacier

Chang Woo Lee[1,2], Sun-Ha Park[1], Chang Sook Jeong[1,2], Chang Sup Lee[3], Jong Wook Hong[4,5], Hyun Ho Park[6], Hyun Park[1,2], HaJeung Park[7]* and Jun Hyuck Lee[1,2]*

[1]Unit of Polar Genomics, Korea Polar Research Institute, Incheon 21990, Republic of Korea, [2]Department of Polar Sciences, Korea University of Science and Technology, Incheon 21990, Republic of Korea, [3]College of Pharmacy and Research Institute of Pharmaceutical Sciences, Gyeongsang National University, Jinju 52828, Republic of Korea, [4]Department of Bionanotechnology, Graduate School, Hanyang University, Seoul 04763, Republic of Korea, [5]Department of Bionanoengineering, Hanyang University, Kyunggi-do 15588, Republic of Korea, [6]College of Pharmacy, Chung-Ang University, 84 Heukseok-ro, Dongjak, Seoul 06974, Republic of Korea, [7]X-Ray Core, TRI, The Scripps Research Institute, Jupiter, FL 33458, USA

*Correspondence: hajpark@scripps.edu, junhyucklee@kopri.re.kr

Spo0F is a response regulator that modulates sporulation, undergoes phosphorylation for phosphorelay signal transduction, and interacts with various regulatory proteins; however, the mechanisms through which phosphorylation induces structural changes and regulates interactions with binding partners remain unclear. Here, we determined the unphosphorylated crystal structure of Spo0F from the psychrophilic bacterium *Paenisporosarcina* sp. TG-14 (*Pa*Spo0F) and established a phosphorylation-state structural model. We found that *Pa*Spo0F underwent structural changes (Lys54 and Lys102) by phosphorylation and generated new interactions (Lys102/Gln10 and Lys54/Glu84) to stabilize the β4/α4 and β1/α1 loop structures, which are important target-protein binding sites. Analysis of *Bacillus subtilis* Spo0 variants revealed movement by *Bs*Spo0F Thr82 and Tyr84 residues following interaction with *Bs*Spo0B, providing insight into the movement of corresponding residues in *Pa*Spo0F (Thr80 and Tyr82), with further analysis of *Bs*Spo0F/*Bs*RapH interaction revealing alterations in the β4/α4 loop region. These results suggest that phosphorylation-induced structural rearrangement might be essential for *Pa*Spo0F activation and expand the understanding of Spo0F-specific activation mechanisms during sporulation.

INTRODUCTION

Sporulation is a crucial survival strategy for some microorganisms, such as *Bacillus*, *Clostridium*, and *Sporosarcina* spp. In harsh environments, microorganisms enter a dormant state and generate a coat that comprises several layers. These morphological and physiological changes allow microorganisms to survive in the presence of environmental stressors, such as heat, cold, dryness, ultraviolet radiation, and insufficient nutrients (Al-Hinai et al., 2015; Desnous et al., 2009; Nicholson et al., 2000; Roszak and Colwell, 1987). The psychrophilic bacterium *Paenisporosarcina* sp. TG-14 was isolated from sediment-laden, stratified basal ice from Taylor Glacier, McMurdo Dry Valley, Antarctica (Koh et al., 2012). *Paenisporosarcina* sp. TG-14 is thought to have survived in an extremely cold environment for a long time by inducing spore formation.

During the initial stage of sporulation, signal pathways are managed by an expanded two-component system called a phosphorelay (Stephenson and Hoch, 2002), with the signal originating at a sporulation histidine kinase (e.g., KinA, KinB, KinC, KinD, and KinE) via autophosphorylation (Brunsing et al., 2005; Jiang et al., 2000; LeDeaux and Grossman, 1995; LeDeaux et al., 1995; Stephenson and Hoch, 2001). Notably, environmental signals can be triggers for these pathways. Next, the phosphohistidine in the kinase domain of the sporulation histidine kinase transfers the phosphoryl group to Spo0F (Jiang et al., 2000; Lee et al., 2008), in which an aspartate residue is phosphorylated, thereby promoting Spo0F interaction with Spo0B. Spo0B is then phosphorylated by Spo0F, after which Spo0B phosphorylates the regulatory domain of Spo0A (Burbulys et al., 1991; Tzeng et al., 1998; Varughese et al., 2006). Phosphorylated Spo0A then forms a dimer that binds to 0A boxes and/or specific DNA sequences to activate the transcription of downstream spore-forming genes (Ireton et al., 1993; Lewis et al., 2002; Muchova et al., 2004).

Spo0F is a single-domain protein homologous to the N-terminal activator domain of response regulators (Feher et al., 1997; Zapf et al., 1996). Spo0F belongs to the CheY-like protein

superfamily, and CheY is a member of the response-regulator family in bacterial two-component signaling systems (Volz, 1993). Nitrate/Nitrite-response regulator, nitrogen regulatory protein, ethylene receptor, and Spo0A also belong to the CheY-like superfamily (Baikalov et al., 1996; Lee et al., 2003; Lewis et al., 1999; Müller-Dieckmann et al., 1999). The compact globular protein Spo0F has a β5/α5-barrel scaffold architecture with one divalent ion at the active site (Mukhopadhyay et al., 2004). Moreover, an aspartate in the Spo0F active site is phosphorylated by sporulation histidine kinases and acts as a phosphate donor for the histidine receptor on Spo0B (Varughese et al., 2006). Phosphorylated Spo0F can be dephosphorylated by Rap phosphatase (Parashar et al., 2011), with the formation and destruction of the phosphorylated (active) signaling molecule tightly controlled for successful signal transduction.

In this study, we elucidated the molecular basis of Spo0F-mediated phosphorelay by determining the X-ray crystal structure of unphosphorylated Spo0F from the psychrophilic bacterium *Paenisporosarcina* sp. TG-14 (*Pa*Spo0F) and generating a phosphorylated structural model of *Pa*Spo0F. Our findings provide important insights into the activation mechanism of *Pa*Spo0F.

RESULTS AND DISCUSSION

Protein expression and crystallization of *Pa*Spo0F

Recombinant PaSpo0F was expressed and purified to apparent homogeneity, with purified PaSpo0F displaying a homogenous band with a molecular mass of ~11 kDa according to sodium dodecyl sulfate polyacrylamide gel electrophoresis (SDS-PAGE) (Figure 1A). Analytical ultracentrifugation performed to determine the oligomeric state of PaSpo0F resulted in a sedimentation-coefficient distribution confirming that inactive (unphosphorylated) PaSpo0F existed as a monomer with a corresponding molecular mass of 11.8 kDa (Figure 1B). The purified PaSpo0F protein was subsequently concentrated to 12.8 mg/mL for crystallization, trials of which were performed at 293 K using the sitting-drop vapor diffusion method. A Mosquito crystallization robot (TTP Labtech, Melbourn, UK) was used to screen >980 different conditions. The stacked plate-shaped crystals of PaSpo0F appeared within 2 days under the following conditions: 40% (v/v) polyethylene glycol (PEG) 300, 100 mM sodium carcodylate/HCl (pH 6.5), and 200 mM calcium acetate. Crystals were ~200 × ~50 × ~100 μm in size (Figure 1C). Crystals were harvested and soaked in paratone-N oil for cryoprotection under a stream of liquid nitrogen. An X-ray diffraction dataset with 180 images at 1.8 Å resolution limit was successfully collected.

Overall structure of unphosphorylated *Pa*Spo0F

The crystal structure of *Pa*Spo0F was determined at 1.8 Å resolution in space group $P2_12_12_1$, with one molecule in the asymmetric unit. The final structural model was refined to an R_{work} value of 18.8% and an R_{free} value of 22.6%. The overall structure of PaSpo0F had a single compact $(\alpha/\beta)_5$-fold domain similar to the receiver-domain structure of CheY-like superfamily proteins (Galperin, 2006). Five β-strands formed a parallel β-sheet, with five α-helices surrounding the β-sheet (Figure 2A). A search for structural homologs using the DALI server revealed that the closest PaSpo0F homolog was Spo0F from *Bacillus subtilis* (*Bs*Spo0F) (Holm and Sander, 1995; Varughese et al., 2006;

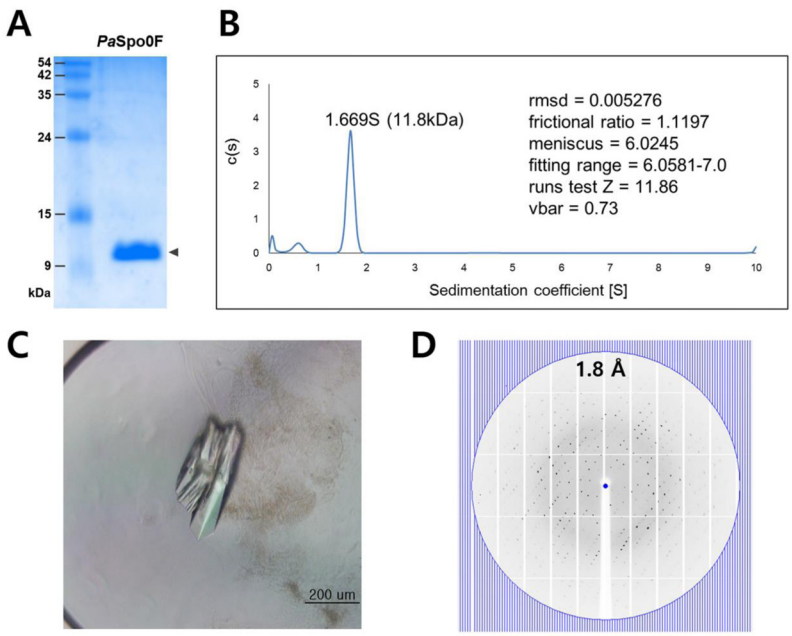

FIGURE 1 | Recombinant *Pa*Spo0F purification, crystallization, and X-ray diffraction data collection. (A) Purified *Pa*Spo0F protein (3.2 μg) was visualized using 12.5% SDS-PAGE. (B) Analytical ultracentrifugation experiments using 0.5 mg/mL *Pa*Spo0F yielded a mass of ~11.8 kDa (sedimentation coefficient: 1.669 S; frictional ratio: 1.1197), indicating that *Pa*Spo0F was a monomer in solution. (C) Crystals of *Pa*Spo0F used for X-ray diffraction data collection. (D) A representative X-ray diffraction pattern of the *Pa*Spo0F crystal, with a maximum resolution limit of 1.8 Å.

Zapf et al., 2000), with the YycF receiver domain, NtrX receiver domain, and CheY also returning high DALI scores (Table 1) (Fernández et al., 2015; Usher et al., 1998). PaSpo0F shared 65% sequence identity with *Bs*Spo0F, and unphosphorylated PaSpo0F showed high structural similarity to unphosphorylated *Bs*Spo0F (PDB: 1PEY), with a root mean square deviation (r.m.s.d.) of 1.184 Å for 114 Cα atoms (Mukhopadhyay et al., 2004). Minor structural differences were observed in the loop

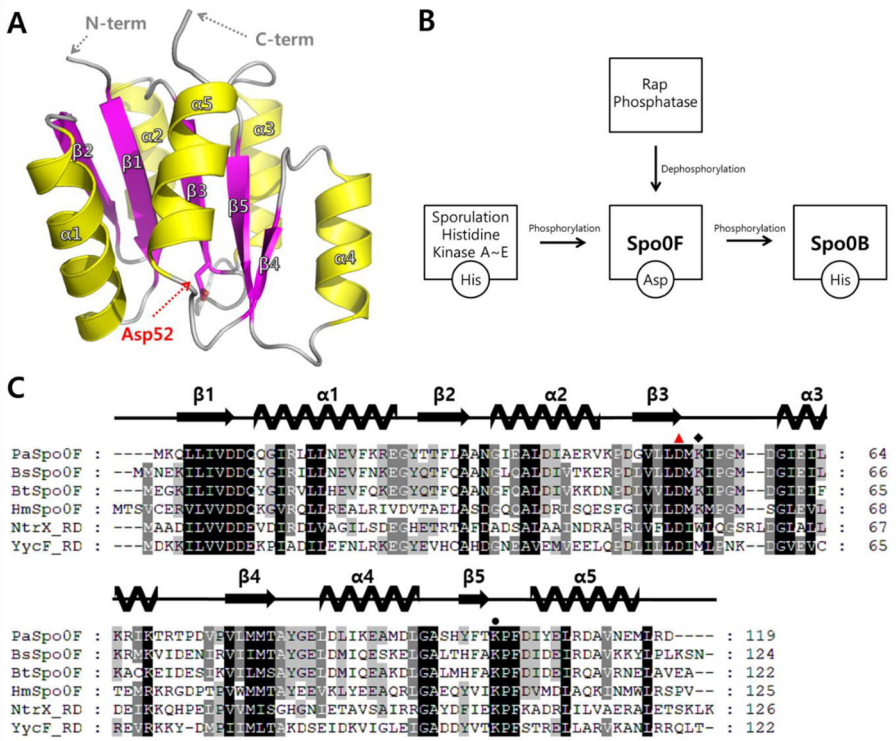

FIGURE 2 | Crystal structure of *Pa*Spo0F and sequence alignment with other response-regulator proteins. (A) The overall structure of *Pa*Spo0F is drawn as a ribbon diagram with α-helices colored yellow and β-strands colored magenta. (B) A simplified scheme for phosphoryl signal transduction by Spo0F. (C) Multiple sequence alignments of *Pa*Spo0F (NCBI reference sequence number: WP_017382123.1), *Bs*Spo0F (Uniprot code: P06628; PDB: 1NAT), Spo0F from *Bacillus thuringiensis* (Uniprot code: P52942), Spo0F from *Heliobacillus mobilis* (Uniprot code: Q0PIJ8), the NtrX receiver domain (1–126; Uniprot code: Q2YPW6; PDB: 4D6X), and the YycF receiver domain (1–122; Uniprot code: P37478; PDB: 2ZWM). The phosphorylated residue (Asp52) is indicated with a red triangle, and Lys54 and Lys102 are indicated by a black rhombus and a black circle, respectively. The multiple sequence alignment was performed with ClustalX (http://www.clustal.org/clustal2/) and edited with GeneDoc (http://iubio.bio.indiana.edu/soft/molbio/ibmpc/genedoc-readme.html).

TABLE 1 | Structural homologs of *Pa*Spo0F according to DALI search results (DALI-Lite server)

Protein	PDB code	DALI Z-score	UniProtKB code	Sequence %ID with *Pa*Spo0F (aligned residue number)	Reference
Beryllofluoride-bound Spo0F in complex with Spo0B	2FTK	24.5	P06628	62% (119)	(Varughese et al., 2006)
Spo0F in complex with Spo0B	1F51	23.2	P06628	63% (119)	(Zapf et al., 2000)
YycF receiver domain	2ZWM	23.0	P37478	35% (118)	Not yet published
*Bs*Spo0F	1NAT	22.9	P06628	63% (119)	(Madhusudan et al., 1997)
RapH in complex with Spo0F	3Q15	22.7	P06628	65% (116)	(Parashar et al., 2011)
Mn^{2+}-bound Spo0F	1PEY	22.7	P06628	63% (119)	(Mukhopadhyay et al., 2004)
NtrX receiver domain from *Brucella abortus*	4D6X	22.5	Q2YPW6	30% (117)	(Fernández et al., 2015)
Phosphatase-resistant Spo0F mutant	1SRR	22.5	P06628	63% (119)	(Zapf et al., 1996)
CheY from *Thermotoga maritima*	4QYW	22.4	Q56312	32% (117)	Not yet published
Putative response regulator from *Chloroflexus aurantiacus*	3T6K	22.3	A9WCL5	34% (119)	Not yet published
CheY from *Thermotoga maritima*	3TMY	22.3	Q56312	33% (116)	(Usher et al., 1998)

region of the neighboring active site, where one magnesium ion was bound tightly in PaSpo0F via interactions with side chains of Asp8, Asp9, and Asp52 and the main chain carbonyl oxygen of Lys54. The predicted phosphorylation site (Asp52) in PaSpo0F (Asp54 in *Bs*Spo0F) is highly conserved in Spo0F proteins (Figure 2C).

Comparison with other receiver-domain-containing proteins

Structural superposition with the receiver domain of NtrX (PDB: 4D6X) from *Brucella abortus* showed clear differences in the phosphorylation site (Fernández et al., 2015) (Figure 3A). In the NtrX structure, Lys54 and Pro56 of PaSpo0F located on the β3/α3 loop region are substituted by Trp55 and Gln57, respectively. Moreover, NtrX has a slightly longer β3/α3 loop region than PaSpo0F, and PaSpo0F Gln10 and Tyr84 residues are substituted by Glu11 and His85, respectively. Additionally, structural comparison with the receiver domain of YycF (PDB: 2ZWM) from *B. subtilis* revealed striking differences in the phosphorylation site (Figure 3B), where Gln10, Lys54, Tyr82, and Gly83 of PaSpo0F were substituted by Glu10, Met54, Lys80, and Asp82, respectively, and large variations were observed between the β4/α4 loop region. However, we noted that the phosphorylation site at Asp52 was conserved in all structures. The conserved residues Asp8, Asp9, and Lys102 in PaSpo0F play a central role in phosphorylation, and each analyzed structure displayed combinations of various residues near the phosphorylation site, resulting in different charge distributions and physical structures. These findings suggest that these features confer variable specificity in protein-protein interactions.

Structural modeling of phosphorylated *Pa*Spo0F

The active state (phosphorylated) of Spo0F has a short half-life (several hours in the case of *Bs*Spo0F) due to autodephosphorylation, which hampers structure analysis of phosphorylated Spo0F (Perego, 2001; Thomas et al., 2008). Therefore, a phosphorylated (active state) PaSpo0F model was generated by molecular modeling, followed by energy minimization based on our apo (inactive state) PaSpo0F structure as a template to obtain further insights into the activation mechanism and target-protein recognition. The modeling data

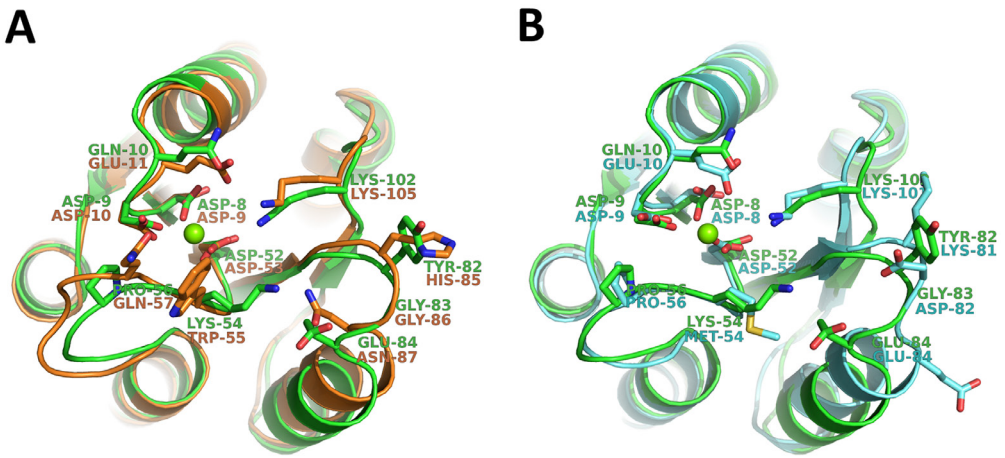

FIGURE 3 | Structural comparison with other receiver-domain-containing proteins. (A) Structural superimposition of *Pa*Spo0F (green) and the NtrX receiver domain (tvorange). (B) Structural superimposition of *Pa*Spo0F (green) and the YycF receiver domain (aquamarine). The residues located in proximity to the phosphorylation site are shown as stick models. The magnesium ion bound by *Pa*Spo0F is presented as a light-green sphere.

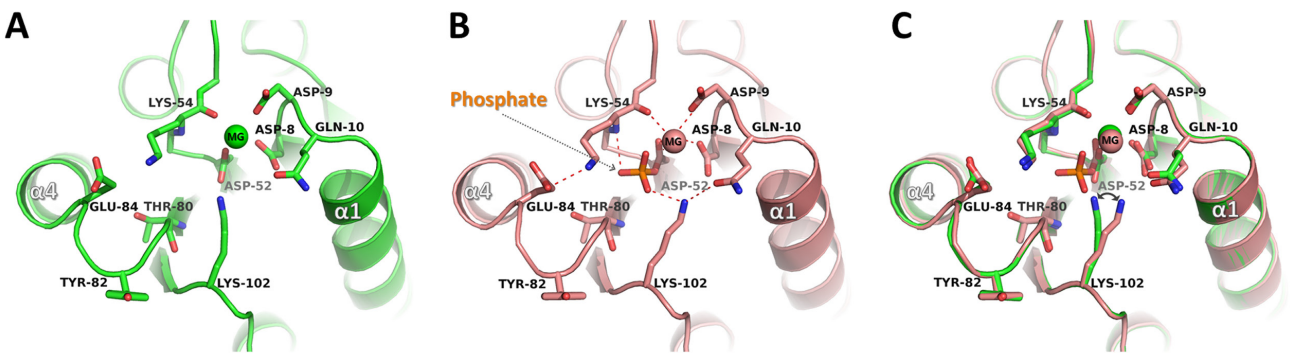

FIGURE 4 | Structural comparison of unphosphorylated (X-ray crystal structure; inactive state) and phosphorylated (modelled structure; active state) *Pa*Spo0F. (A) Crystal structure of unphosphorylated *Pa*Spo0F. (B) Modelled structure of phosphorylated *Pa*Spo0F. (C) Structural superposition of unphosphorylated *Pa*Spo0F (green) and phosphorylated *Pa*Spo0F (salmon). The bound magnesium ion is presented as a sphere, and several residues important for target protein binding (Tyr82), metal binding (Asp8, Asp9, and Asp52), phosphate interaction (Lys54 and Lys102), and loop stabilization (Glu84 and Gln10) are shown as stick models. Phosphorylation of *Pa*SPo0F changed the interaction network proximal to the phosphate- and metal-binding sites.

showed that the negatively charged phosphate group was stabilized by the magnesium ion, the NZ atom of the Lys102 side chain, and the nitrogen backbone atom of Lys54.

As shown in Figure 4, structural changes in Lys54 and Lys102 were detected after phosphorylation. Additionally, these results indicated that phosphorylation at Asp52 induced rearrangement of the polypeptide backbone of Lys54 and movement of the Lys102 side chain, which was rotated to an alternative conformation in phosphorylated PaSpo0F and formed a new hydrogen bond (3.4 Å) with the NE2 atom of Gln10 (located in the β1/α1 loop region). Moreover, Lys54 formed a new salt bridge with Glu84 (located in the β4-α4 loop region) in the phosphorylated PaSpo0F model.

The functional importance of the β4/α4 loop and the α1 helix in Spo0F has been discussed previously (Feher and Cavanagh, 1999; Hoch and Varughese, 2001; Jiang et al., 1999). Spo0F is involved in the phosphorelay system, which controls sporulation initiation. Moreover, Spo0F is phosphorylated by sporulation histidine kinases and subsequently phosphorylates Spo0B. Inversely, Spo0F is dephosphorylated by RapH for its inactivation (Figure 2B). Previous studies revealed the complex structures of beryllofluoride-bound *Bs*Spo0F and *Bs*Spo0B (PDB: 2FTK). Our structural comparison of apo PaSpo0F with *Bs*Spo0B-bound *Bs*Spo0F revealed a 51.6° rotation of the Thr82 side chain in *Bs*Spo0F, with the corresponding residue in PaSpo0F (Thr80) rotated toward the bound beryllium fluoride (a phosphate analog) to promote interaction. Additionally, we observed rotational movement of the Tyr84 side chain of *Bs*Spo0F (corresponding to Tyr82 in PaSpo0F) to allow a hydrophobic interaction with the side chain CG and CD atoms of Lys63 in *Bs*Spo0B. As a result, these interactions induced a longer β4 strand (residues 76–81) in *Bs*Spo0B-bound *Bs*Spo0F than that (residues 76–80) in the apo structure of PaSpo0F. These conformational changes might promote phosphate transfer from Asp52 of PaSpo0F to the histidine residue of Spo0B (Figure 5A). To analyze mechanisms associated with Spo0F dephosphorylation by RapH, we compared our structure with *Bs*Spo0F–*Bs*RapH complex crystal structure determined by Vijay et al. (PDB: 3Q15). We observed conformational changes in the β4/α4 loop of *Bs*Spo0F, with this loop flipped toward the active site, and the Tyr84 residue located in the β4/α4 loop shifted toward the α3 helix of *Bs*RapH. These conformational changes promoted interaction with *Bs*RapH, thereby allowing the Gln47 of *Bs*RapH to dephosphorylate Asp54 (corresponding to Asp52 in PaSpo0F) of *Bs*Spo0F (Figure 5B).

Although several small conformational changes were detected, phosphorylation did not induce large conformational changes in the PaSpo0F structure. Superposition of Cα atoms from unphosphorylated PaSpo0F with the phosphorylated PaSpo0F model structure yielded r.m.s.d. values of 0.114 over 111 Cα atoms. Previous results showed that the RapH phosphatase is capable of interacting with both phosphorylated and unphosphorylated *Bs*Spo0F, though it exhibits stronger affinity for phosphorylated *Bs*Spo0F (Bongiorni et al., 2006; Gardino et al., 2003; Ishikawa et al., 2002). These findings indicated that while Spo0F phosphorylation did not induce significant conformational changes, structural alterations still occurred.

METHODS

Cloning, protein expression, and purification

The DNA fragments encoding full-length Spo0F (residues 1–119) from *Paenisporosarcina* sp. TG-14 were synthesized with codon optimization for expression in *Escherichia coli* (BIONEER Inc., Daejeon, Korea). The DNA fragments were cloned into the expression vector pET-28a (Nocagen, Madison, WI, USA) using *Nde*I and *Xho*I restriction sites. The final constructs containing a hexahistidine tag, a thrombin-cleavage site, and the target gene under the control of the T7 promoter were transformed into *E. coli* strain BL21(DE3) (Enzynomics, Daejeon, Korea) for expression. The cells were grown in LB medium supplemented with kanamycin (50 μg/mL) at 37°C until reaching an OD_{600} of 0.6. Overexpression of *Pa*Spo0F was induced by the addition of 0.5 mM isopropyl-1-thio-β-D-galctopyranoside at 25°C overnight. The cells were harvested by centrifugation (VS-24SMTi; Vision Scientific, Bucheon, Republic of Korea) at 6,000 rpm and 4°C for 20 min. The harvested cell pellets were suspended in buffer [50 mM sodium phosphate, 300 mM NaCl, 5 mM imidazole (pH 8.0), and 0.2 mg/mL lysozyme]. The cells were lysed using an ultrasonicator (VCX 750; Sonics & Materials, Newtown, CT, USA), and the lysates were clarified by

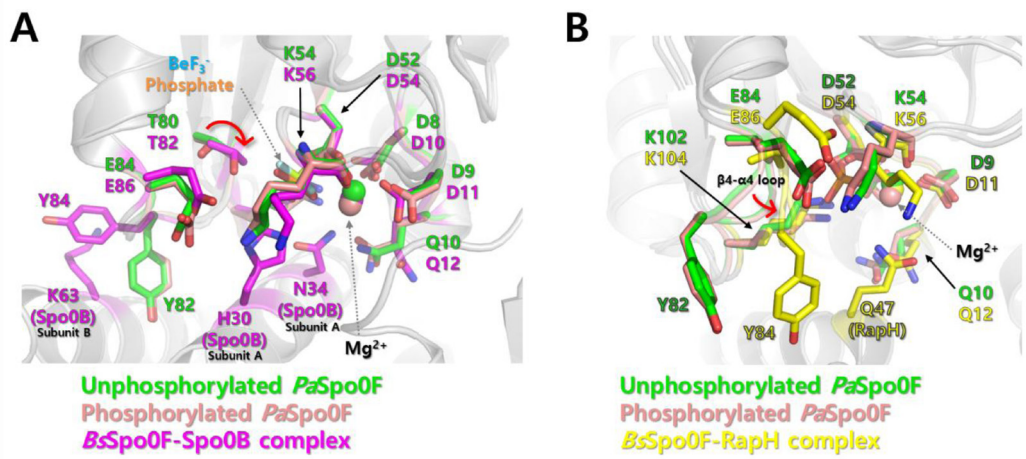

FIGURE 5 | Interaction mode of Spo0F with Spo0B or RapH. (A) Structural superposition of unphosphorylated *Pa*Spo0F (green) and Spo0B-bound *Bs*Spo0F (magenta), indicating that Thr80 undergoes conformational changes during phosphate transfer from Spo0F to Spo0B. (C) Structural superposition of unphosphorylated *Pa*Spo0F (green) and RapH-bound *Bs*Spo0F (yellow), indicating that Thr80 and Tyr82 undergo major conformational changes following RapH binding. Notably, Gln47 of RapH interacts with Gln10 of *Pa*Spo0F.

centrifugation at 16,000 rpm for 40 min at 4°C. The supernatants were loaded onto pre-equilibrated Ni-NTA columns (Qiagen, Hilden, Germany), which were washed with wash buffer [50 mM sodium phosphate, 300 mM NaCl, and 20 mM imidazole (pH 8.0)] and eluted with elution buffer [50 mM sodium phosphate, 300 mM NaCl, and 300 mM imidazole (pH 8.0)]. The hexahistidine tag was cleaved using thrombin at 4°C overnight. *Pa*Spo0F was further purified by gel filtration on a Superdex 200 column (GE Healthcare, Piscataway, NJ, USA) equilibrated with 20 mM Tris-HCl (pH 8.0) and 150 mM NaCl. Fractions containing PaSpoF were collected and concentrated to 12.8 mg/mL using Amicon Ultra-15 centrifugal filters (Ultracel-10 K; Merck Millipore Ltd., Cork, Ireland). Protein concentration and purity were measured using a Nanodrop spectrophotometer (NanoDrop Technologies, Wilmington, DE, USA).

*Pa*Spo0F crystallization

Initial crystallization screening was performed in 96-well crystallization plates (Emerald Bio, Bainbridge Island, WA, USA) at 293 K using the sitting-drop vapor-diffusion method. Several commercially available screening kits [MCSG I-IV (Microlytic, Burlington, MA, USA), SG1 screen (Molecular Dimensions, Maumee, OH, USA), Wizard classic 1-4 (Emerald Bio), SaltRx, PEG/Ion and Index (Hampton Research, Aliso Viejo, CA, USA)] were used with a Mosquito crystallization robot (TTP Labtech, UK). The crystallization drops comprised equal volumes of protein solution (0.2 μL) and crystallization reservoir solution (0.2 μL). Crystals of *Pa*Spo0F were obtained from conditions of 40% (v/v) PEG 300, 100 mM sodium carcodylate/HCl (pH 6.5), and 200 mM calcium acetate (Wizard classic 3-4 #E11; Emerald Bio) after 2 days of incubation at 293 K. To obtain larger crystals, the hanging-drop vapor-diffusion method was performed in 24-well crystallization plates (Molecular Dimensions) at 293 K. The crystallization drop size was increased by mixing 1 μL of protein solution and 1 μL of reservoir solution, and the reservoir volume was increased to 500 μL. Single diffraction-quality crystals of *Pa*Spo0F were obtained after 2 days of incubation at 293 K.

TABLE 2 | Data collection and refinement statistics

Dataset	*Pa*Spo0F
X-ray source	PAL 5C beam line
Space group	$P2_12_12_1$
Wavelength (Å)	0.97940
Resolution (Å)	50.00–1.80 (1.83–1.80)
Total reflections	57616
Unique reflections	9571 (477)
Average I/σ (I)	27.9 (2.0)
R_{merge} [a]	0.097 (0.614)
Redundancy	6.0 (5.6)
Completeness (%)	99.5 (100.0)
Refinement	
Resolution range (Å)	39.75–1.80 (1.85–1.80)
No. of reflections of working set	9045 (655)
No. of reflections of test set	487 (40)
No. of amino acid residues	119
No. of water molecules	43
R_{cryst} [b]	0.188 (0.238)
R_{free} [c]	0.226 (0.310)
R.m.s. bond length (Å)	0.011
R.m.s. bond angle (°)	1.576
Average B-value (Å^2) (protein)	34.703
Average B-value (Å^2) (solvent)	39.137

[a] $R_{merge} = \Sigma \mid <I> - I \mid / \Sigma <I>$.
[b] $R_{cryst} = \Sigma \mid |Fo| - |Fc| \mid / \Sigma |Fo|$.
[c] R_{free} calculated using 5% of all reflections excluded from refinement stages using high-resolution data.
Values in parentheses refer to the highest resolution shells.

Data collection and structure determination

Single crystals were harvested and quickly soaked in N-paratone oil (Hampton Research) and flash-cooled in a liquid-nitrogen stream at 100 K. X-ray diffraction data were collected on a BL-5C beam line at the Pohang Accelerator Laboratory (Pohang, Korea). The dataset with a maximum 1.8 Å resolution containing 180 images with 1° rotation was indexed, integrated, and scaled using HKL-2000 (Otwinowski and Minor, 1997). The crystals belonged to space group $P2_12_12_1$, with unit-cell parameters a = 29.518 Å, b = 49.361 Å, and c = 67.067 Å. The Matthews coefficient was 1.88 Å^{3}Da^{-1}, and the solvent content was 34.59% (Matthews, 1968). The *Pa*Spo0F structure was determined by the molecular replacement method using *MOLREP* from the *CCP4i* suite (Vagin and Teplyakov, 1997; Winn et al., 2011). *Bs*Spo0F (PDB: 1PUX) was used as the initial search model (Gardino et al., 2003). Successive refinement and model building were performed manually using *REFMAC5*, *COOT*, and *PHENIX* (Adams et al., 2010; Emsley and Cowtan, 2004; Murshudov et al., 2011), and the final model was checked with *Molprobity* (Chen et al., 2010). Detailed data collection and refinement statistics are summarized in Table 2. The coordinates and structure factors of *Pa*Spo0F were deposited in the RCSB Protein Data Bank under accession code 6IFH. All structural representations were rendered using *PyMOL* (DeLano, 2002).

Structural modeling of the *Pa*Spo0F phosphorylated-state

The structural model of phosphorylated *Pa*Spo0F was prepared using Maestro version 9.5 software (Schrodinger, Portland, OR, USA) by adding a phospho-aspartate residue at Asp52. Conformational scanning was conducted using the MacroModel program (Schrodinger) in order to identify the lowest energy conformation. The final model was energy minimized using Prime version 3.1 (Schrodinger).

CONFLICT OF INTEREST

The authors declare no potential conflicts of interest.

ACKNOWLEDGEMENTS

We would like to thank the staff at the X-ray core facility of Korea Basic Science Institute (KBSI; Ochang, Korea) and BL-5C of the Pohang Accelerator Laboratory (Pohang, Korea) for their kind help in data collection. This work was supported by the Korea Polar Research Institute (KOPRI; grant No. PE18210 and PE19210 to JHL) and by the Basic Science Research Program 2018R1A2B6005354 through the National Research Foundation of Korea (NRF) funded by the Ministry of Science, ICT and Future Planning of Korea.

Original Submission: Nov 1, 2018
Revised Version Received: Dec 11, 2018
Accepted: Dec 15, 2018

REFERENCES

Adams, P.D., Afonine, P.V., Bunkóczi, G., Chen, V.B., Davis, I.W., Echols, N., Headd, J.J., Hung, L.-W., Kapral, G.J., Grosse-Kunstleve, R.W., McCoy, A.J., Moriarty, N.W., Oeffner, R., Read, R.J., Richardson, D.C., et al. (2010). PHENIX: a comprehensive Python-based system for macromolecular structure solution. *Acta Crystallogr D Biol Crystallogr* **66**, 213-221.

Al-Hinai, M.A., Jones, S.W., and Papoutsakis, E.T. (2015). The *Clostridium*

sporulation programs: diversity and preservation of endospore differentiation. *Microbiol Mol Biol Rev* **79**, 19-37.

Baikalov, I., Schröder, I., Kaczor-Grzeskowiak, M., Grzeskowiak, K., Gunsalus, R.P., and Dickerson, R.E. (1996). Structure of the Escherichia coli response regulator NarL. *Biochemistry* **35**, 11053-11061.

Bongiorni, C., Stoessel, R., Shoemaker, D., and Perego, M. (2006). Rap phosphatase of virulence plasmid pXO1 inhibits *Bacillus anthracis* sporulation. *J Bacteriol* **188**, 487-498.

Brunsing, R.L., La Clair, C., Tang, S., Chiang, C., Hancock, L.E., Perego, M., and Hoch, J.A. (2005). Characterization of sporulation histidine kinases of *Bacillus anthracis*. *J Bacteriol* **187**, 6972-6981.

Burbulys, D., Trach, K.A., and Hoch, J.A. (1991). Initiation of sporulation in B. subtilis is controlled by a multicomponent phosphorelay. *Cell* **64**, 545-552.

Chen, V.B., Arendall, W.B., Headd, J.J., Keedy, D.A., Immormino, R.M., Kapral, G.J., Murray, L.W., Richardson, J.S., and Richardson, D.C. (2010). MolProbity: all-atom structure validation for macromolecular crystallography. *Acta Crystallogr D Biol Crystallogr* **66**, 12-21.

DeLano, W.L. (2002). The PyMOL molecular graphics system. Available at: www.pymol.org.

Desnous, C., Guillaume, D., and Clivio, P. (2009). Spore photoproduct: a key to bacterial eternal life. *Chem Rev* **110**, 1213-1232.

Emsley, P., and Cowtan, K. (2004). Coot: model-building tools for molecular graphics. *Acta Crystallogr D Biol Crystallogr* **60**, 2126-2132.

Feher, V.A., and Cavanagh, J. (1999). Millisecond-timescale motions contribute to the function of the bacterial response regulator protein Spo0F. *Nature* **400**, 289.

Feher, V.A., Zapf, J.W., Hoch, J.A., Whiteley, J.M., McIntosh, L.P., Rance, M., Skelton, N.J., Dahlquist, F.W., and Cavanagh, J. (1997). High-resolution NMR structure and backbone dynamics of the Bacillus subtilis response regulator, Spo0F: implications for phosphorylation and molecular recognition. *Biochemistry* **36**, 10015-10025.

Fernández, I., Otero, L.H., Klinke, S., del Carmen Carrica, M., and Goldbaum, F.A. (2015). Snapshots of conformational changes shed light into the NtrX receiver domain signal transduction mechanism. *J Mol Biol* **427**, 3258-3272.

Galperin, M.Y. (2006). Structural classification of bacterial response regulators: diversity of output domains and domain combinations. *J Bacteriol* **188**, 4169-4182.

Gardino, A.K., Volkman, B.F., Cho, H.S., Lee, S.-Y., Wemmer, D.E., and Kern, D. (2003). The NMR solution structure of BeF3−-activated Spo0F reveals the conformational switch in a phosphorelay system. *J Mol Biol* **331**, 245-254.

Hoch, J.A., and Varughese, K. (2001). Keeping signals straight in phosphorelay signal transduction. *J Bacteriol* **183**, 4941-4949.

Holm, L., and Sander, C. (1995). Dali: a network tool for protein structure comparison. *Trends Biochem Sci* **20**, 478-480.

Ireton, K., Rudner, D.Z., Siranosian, K.J., Grossman, A.D. (1993). Integration of multiple developmental signals in *Bacillus subtilis* through the Spo0A transcription factor. Genes Dev **7**, 283-294.

Ishikawa, S., Core, L.J., and Perego, M. (2002). Biochemical characterization of aspartyl-phosphate phosphatase interaction with a phosphorylated response regulator and its inhibition by a pentapeptide.

Jiang, M., Shao, W., Perego, M., and Hoch, J. (2000). Multiple histidine kinases regulate entry into stationary phase and sporulation in *Bacillus subtilis*. *Mol Microbiol* **38**, 535-542.

Jiang, M., Tzeng, Y.L., Feher, V.A., Perego, M., and Hoch, J. (1999). Alanine mutants of the Spo0F response regulator modifying specificity for sensor kinases in sporulation initiation. *Mol Microbiol* **33**, 389-395.

Koh, H.Y., Lee, S.G., Lee, J.H., Doyle, S., Christner, B.C., and Kim, H.J. (2012). Draft genome sequence of Paenisporosarcina sp. strain TG-14, a psychrophilic bacterium isolated from sediment-laden stratified basal ice from Taylor Glacier, McMurdo Dry Valleys, Antarctica. *J Bacteriol* **194**, 6656-6657.

LeDeaux, J.R., and Grossman, A.D. (1995). Isolation and characterization of kinC, a gene that encodes a sensor kinase homologous to the sporulation sensor kinases KinA and KinB in *Bacillus subtilis*. *J Bacteriol* **177**, 166-175.

LeDeaux, J.R., Yu, N., and Grossman, A.D. (1995). Different roles for KinA, KinB, and KinC in the initiation of sporulation in *Bacillus subtilis*. *J Bacteriol* **177**, 861-863.

Lee, J., Tomchick, D.R., Brautigam, C.A., Machius, M., Kort, R., Hellingwerf, K.J., and Gardner, K.H. (2008). Changes at the KinA PAS-A dimerization interface influence histidine kinase function. *Biochemistry* **47**, 4051-4064.

Lee, S.-Y., De La Torre, A., Yan, D., Kustu, S., Nixon, B.T., and Wemmer, D.E. (2003). Regulation of the transcriptional activator NtrC1: structural studies of the regulatory and AAA+ ATPase domains. *Genes Dev* **17**, 2552-2563.

Lewis, R.J., Brannigan, J.A., Muchová, K.n., Barák, I., and Wilkinson, A.J. (1999). Phosphorylated aspartate in the structure of a response regulator protein1. *J Mol Biol* **294**, 9-15.

Lewis, R.J., Scott, D.J., Brannigan, J.A., Ladds, J.C., Cervin, M.A., Spiegelman, G.B., Hoggett, J.G., Barák, I., and Wilkinson, A.J. (2002). Dimer formation and transcription activation in the sporulation response regulator Spo0A1. *J Mol Biol* **316**, 235-245.

Madhusudan, Zapf, J., Hoch, J.A., Whiteley, J.M., Xuong, N.H., and Varughese, K.I. (1997). A response regulatory protein with the site of phosphorylation blocked by an arginine interaction: crystal structure of Spo0F from *Bacillus subtilis*. *Biochemistry* **36**, 12739-12745.

Matthews, B.W. (1968). Solvent content of protein crystals. *J Mol Biol* **33**, 491-497.

Müller-Dieckmann, H.-J., Grantz, A.A., and Kim, S.-H. (1999). The structure of the signal receiver domain of the Arabidopsis thaliana ethylene receptor ETR1. *Structure* **7**, 1547-1556.

Muchova, K., Lewis, R., Perečko, D., Brannigan, J., Ladds, J., Leech, A., Wilkinson, A., and Barák, I. (2004). Dimer-induced signal propagation in Spo0A. *Mol Microbiol* **53**, 829-842.

Mukhopadhyay, D., Sen, U., Zapf, J., and Varughese, K.I. (2004). Metals in the sporulation phosphorelay: manganese binding by the response regulator Spo0F. *Acta Crystallogr D Biol Crystallogr* **60**, 638-645.

Murshudov, G.N., Skubák, P., Lebedev, A.A., Pannu, N.S., Steiner, R.A., Nicholls, R.A., Winn, M.D., Long, F., and Vagin, A.A. (2011). REFMAC5 for the refinement of macromolecular crystal structures. *Acta Crystallogr D Biol Crystallogr* **67**, 355-367.

Nicholson, W.L., Munakata, N., Horneck, G., Melosh, H.J., and Setlow, P. (2000). Resistance of Bacillus endospores to extreme terrestrial and extraterrestrial environments. *Microbiol Mol Biol Rev* **64**, 548-572.

Otwinowski, Z., and Minor, W. (1997). Processing of X-ray diffraction data collected in oscillation mode. In: *Methods in Rnzymology* (Elsevier), pp. 307-326.

Parashar, V., Mirouze, N., Dubnau, D.A., and Neiditch, M.B. (2011). Structural basis of response regulator dephosphorylation by Rap phosphatases. *PLoS Biol* **9**, e1000589.

Perego, M. (2001). A new family of aspartyl phosphate phosphatases targeting the sporulation transcription factor Spo0A of *Bacillus subtilis*. *Mol Microbiol* **42**, 133-143.

Roszak, D., and Colwell, R. (1987). Survival strategies of bacteria in the

natural environment. *Microbiol Rev* **51**, 365.

Stephenson, K., and Hoch, J.A. (2002). Evolution of signalling in the sporulation phosphorelay. *Mol Microbiol* **46**, 297-304.

Stephenson, K., and Hoch, J.A. (2001). PAS-A domain of phosphorelay sensor kinase A: a catalytic ATP-binding domain involved in the initiation of development in *Bacillus subtilis*. *Proc Natl Acad Sci U S A* **98**, 15251-15256.

Thomas, S.A., Brewster, J.A., and Bourret, R.B. (2008). Two variable active site residues modulate response regulator phosphoryl group stability. *Mol Microbiol* **69**, 453-465.

Tzeng, Y.-L., Zhou, X.Z., and Hoch, J.A. (1998). Phosphorylation of the Spo0B response regulator phosphotransferase of the phosphorelay initiating development in *Bacillus subtilis*. *J Biol Chem* **273**, 23849-23855.

Usher, K.C., De La Cruz, A.F.A., Dahlquist, F.W., James Remington, S., Swanson, R.V., and Simon, M.I. (1998). Crystal structures of CheY from *Thermotoga maritima* do not support conventional explanations for the structural basis of enhanced thermostability. *Protein Sci* **7**, 403-412.

Vagin, A., and Teplyakov, A. (1997). MOLREP: an automated program for molecular replacement. *J Appl Cryst* **30**, 1022-1025.

Varughese, K.I., Tsigelny, I., and Zhao, H. (2006). The crystal structure of beryllofluoride Spo0F in complex with the phosphotransferase Spo0B represents a phosphotransfer pretransition state. *J Bacteriol* **188**, 4970-4977.

Volz, K. (1993). Structural conservation in the CheY superfamily. *Biochemistry* **32**, 11741-11753.

Winn, M.D., Ballard, C.C., Cowtan, K.D., Dodson, E.J., Emsley, P., Evans, P.R., Keegan, R.M., Krissinel, E.B., Leslie, A.G., McCoy, A., McNicholas, S.J., Murshudov, G.N., Pannu, N.S., Potterton, E.A., Powell, H.R., et al. (2011). Overview of the CCP4 suite and current developments. *Acta Crystallogr D Biol Crystallogr* **67**, 235-242.

Zapf, J., Sen, U., Hoch, J.A., and Varughese, K.I. (2000). A transient interaction between two phosphorelay proteins trapped in a crystal lattice reveals the mechanism of molecular recognition and phosphotransfer in signal transduction. *Structure* **8**, 851-862.

Zapf, J., Whiteley, J.M., Hoch, J.A., Xuong, N.H., and Varughese, K.I. (1996). Crystal structure of a phosphatase-resistant mutant of sporulation response regulator Spo0F from *Bacillus subtilis*. *Structure* **4**, 679-690.